Carbon deposition by an expanding cascaded arc plasma

CARBON DEPOSITION BY AN EXPANDING CASCADED ARC PLASMA

A.J.M. Buuron, J. J. Beulens, D. C. Schram,
Dept. of Physics, Eindhoven University of Technology,
P.O. Box 513, 5600 MB Eindhoven, The Netherlands

P. Groot, J. Bakker,
Netherlands Energy Research Foundation, ECN,
P.O. Box 1, 1755 ZG Petten, The Netherlands

ABSTRACT

Graphitic materials with various degrees of crystallinity have been deposited by means of an expanding argon/hydrocarbon plasma, with a varying amount of hydrogen admixture. High deposition rates of up to hundreds of nm/s on several cm^2 have been observed. Relations between the deposition parameters, morphology (by Scanning Electron Microscopy), crystallinity (by Raman spectroscopy) and thermal shock resistance of the coatings (by laser heat pulses) have been determined.

INTRODUCTION

The expanding cascaded arc offers a method for the high rate deposition of carbon layers. In the past deposition rates of up to 200 nm/s for a-C:H (amorphous hydrogenated carbon) /1/ and of 10 nm/s for diamond /2/ have been obtained. These rates are an order of magnitude higher than those with the conventional RF or DC glow discharge methods.

Recently the deposition of carbon has been studied as an option for *in situ* repair of erosion damage on the carbon fiber composite (CFC) plasma facing components in the next step fusion reactor NET/ITER (under NET contract no. 90-237). The primary requirements for the coating are a high growth rate and a preferably crystalline character for a good thermomechanical behaviour. Direct diamond deposition on CFC appears to be impossible. The possibility of very fast deposition of nanocrystalline ('amorphous') graphite at hundreds of nm/s by an argon/hydrocarbon plasma has already been reported /3/. In order to optimize the crystallinity of the graphite hydrogen was admixed in the argon/hydrocarbon plasma and also other reactor parameters were varied.

The microstructure of the coatings was analyzed by SEM (Scanning Electron Microscopy) and Raman spectroscopy. At the Netherlands Energy Research Foundation (ECN Petten) disruption simulation experiments with a laser thermal shock set up /4/ were carried out. Direct relations between morphology, crystallinity, erosion resistance and the reactor parameters during deposition are demonstrated.

EXPERIMENTAL

In figure 1. an outline of the expanding cascaded arc set up is shown. The main feature of the method is the separation of the three functions production, transport, and deposition. Principal advantages of this method as compared to the conventional ones are high growth rates by the active particle transport towards the substrate, and flexibility in handling arc and substrate parameters. A cascaded arc plasma (4 mm diameter, 6 cm length), expanding in a vacuum chamber is used as a particle source. Specific features of this source are high power dissipation (about 5 kW), thermal plasma (temperatures ~1 eV) and, a very long continuous operation (days). The carrier gas argon is injected at the beginning of the arc channel (flow rate 100 cc/s), at a pressure in the order of 10^5 Pa. A hydrocarbon (CH_4 or C_2H_2) can be injected (at rates of 0 to 10 cc/s) at the end of the arc channel. As an etching agent hydrogen can be admixed in the middle of the channel. By dissociation and charge exchange a beam of excited species, radicals and ions (Ar, C, H, C_xH_y) is created, expanding supersonically out of the end of the arc channel (the nozzle), into a vacuum chamber (pressure typically 10^2 Pa). After passing through a shock the particles move further toward a substrate at subsonic velocities. A typical value for the carbon ion flux is 10^{19}/s. The total transport time of all particles is relatively small (in the order of 10^{-4} s) and the species ratios in the plasma do not change substantially. More details on reactor and cascaded arc can be found elsewhere /1-3, 5/.

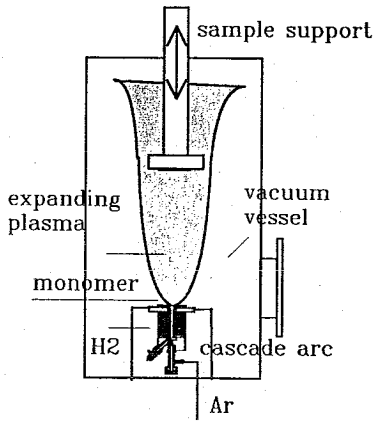

Figure 1. Outline of the expanding cascaded arc set up.

As reported in /3/, the (linear) deposition rate R_d is function of all reactor parameters: the arc power (P), the gas flow rates ({argon}, {hydrocarbon}, {hydrogen}), the type of hydrocarbon (monomer) feed gas, the number of carbon atoms in relation to the arc power (expressed by Q), the chamber pressure p_c, the deposition temperature T_s and the nozzle to substrate distance $d_{n\text{-}s}$. The radial expansion of the beam is governed by diffusion. Its cross section A_b is approximately linear with $d_{n\text{-}s}$ and reciprocal to p_c, see /5/, p. 81. (For $d_{n\text{-}s}$=80 cm and $p_c=10^2$ Pa, $A_b \simeq 120$ cm^2). We define a normalized deposition rate R_n as a measure for the volume deposition rate by dividing the linear deposition rates by p_c: $R_n := R_d/p_c$.

The properties of the deposited graphitic materials were studied primarily in relation to the following deposition conditions /3/:

1. The hydrogen admixture flow rate, mostly expressed as a ratio of fluxes in the expanding beam: {H}/{Ar} and {H}/{C} resp.

2. The inverse energy factor Q = {C}/({Ar}*P_{arc}) (W^{-1})
3. The substrate temperature T_s (°C)

As substrates, 10 mm discs (thickness 5 mm) of carbon fiber composite (CFC, Dunlop DMS 678) with the fiber planes parallel to the surface normal and stainless steel (type AISI 316 Ti) were used. The nozzle-substrate distance was in general 5 cm, resulting in substrate temperatures of about 1000 °C (measured by pyrometry). As a feed gas C_2H_2 was used, as it appears to be more effective for graphite deposition than CH_4. Deposition times were in the order of 20 minutes. Thicknesses and growth rates were estimated by weight change measurements, normalized to a density of 1 g/cm^3.

With a micro Raman set up (Dilor), enabling direct sample inspection, spectra were recorded in a 180° back scattering geometry. As a source the 514.5 nm of an Ar ion laser was used. In general the power was 100 mW and the spot diameter 4 μm^2. Signal recording was done by means of a double (subtractive) monochromator and a diode array. The spectral slit width corresponded to 6.6 cm^{-1}.

The thermal shock tests where performed with a Nd-Yag laser set up. The power density was chosen in the order of the lower NET disruption energy dumps, MJ/m^2 in ms. A description of this test facility can be found elsewhere /4/.

RESULTS AND DISCUSSION

Quantitatively the relation between the crystallinity and the reactor parameters has been analyzed by solving the Raman spectra in Lorentzian components /6/. In fig. 2 it is illustrated that an increasing amount of hydrogen admixture improves the crystallinity of the graphite. The defective graphite peak D at 1355 cm^{-1} and shoulder S at 1621 cm^{-1} decrease strongly with respect to the 1581 cm^{-1} G graphite peak. This result is rather surprising, as it was assumed that in the diamond deposition proces the role of the hydrogen (radicals) was to etch away graphitic carbon. As for diamond deposition, for graphite deposition (or etching) a specific equilibrium environment seems to be determining. The substrate type is also of great importance: increasing the hydrogen admixture (and chamber pressure) to those for diamond deposition on silicon /2/ results in etching of the CFC substrates. In

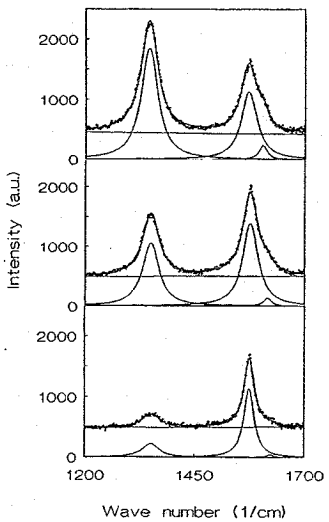

Figure 2. Effect of increasing hydrogen admixture on Raman spectra. From top to bottom H_2 admixtures 5, 10 and 20 cc/s resp.; growth rates 21, 12 and 13 nm/s. Q≃7.10^{-6} W^{-1}, T_s≃ 840 °C.

Table I the optimal values for the three parameters for different types of carbon deposits are summarized. As concerns the other variables, it appears that for the deposition of a coherent graphitic material a high C_2H_2 flow of 8 cc/s (high Q factor) is beneficial. The substrate temperature is high in order to avoid hydrogen incorporation in the the layer and to favor the crystallization (see e.g. /8/). Further no restrictions on the deposition conditions for graphite have been observed.

Table I Summary of required principal deposition conditions for various types of carbon deposits; var = various others; spec. = specific others.

	H_2 admixt. H/Ar	H/C	Q ($10^{-6}W^{-1}$)	p_c (10^2 Pa)	T_s (°C)	substrate
a-C:H /1, 5/	- -	- -	4.1	1	<100	gold, steel (+var.)
amorph. graphite	- -	- -	62	var	>600	CFC, steel (+var?)
cryst. ,,	0.8	5	47	var	800-1400	CFC, steel (+var?)
diamond /2/	2	200	2.6	60	1000	silicon (+spec.?)

The influence of the deposition environment on morphology is shown in figure 3 and 4. Amorphous graphite has a typical columnar cauliflower morphology, while crystalline graphite exhibits a structure with distinct foliates. The crystallite size, estimated from the intensity ratio of the D and the G peak I_d/I_g /7/ increases from ~ 3 to 30 nm. Figure 4 shows that the real graphite packet size is apparently some μms.

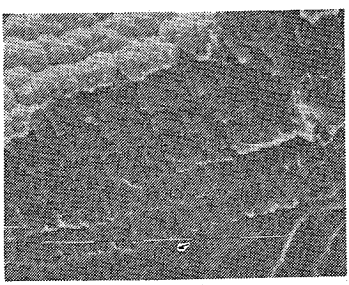

Figure 3. SEM micrograph of a typical amorphous graphite coating (side view). 1 bar = 100 μm.

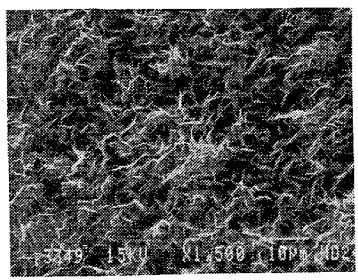

Figure 4. SEM micrograph of a typical crystalline graphite coating (top view), deposited with a hydrogen admixture of 20 cc/s, 1 bar = 10 μm.

In figure 5 the effect of the increasing hydrogen admixture is shown quantitatively. The results of the third diagnostic, the thermal shock testing, can be quantified by the parameter erosion threshold, i.e. the lower limit of the laser pulse power density at which erosion starts to occur. In figures 6 to 8 also the results of accompanying SEM observations are included. Whenever the coating exhibited the foliates structure of crystalline graphite, this is denoted by a full symbol. When the coating had an amorphous graphite or intermediate structure, an open symbol is used. Figure 6 shows that the crystallinity of the coatings and the erosion threshold increase with increasing hydrogen admixture, consistent with the results of the Raman analysis (fig. 5). The deposition rates decrease with increasing hydrogen admixtures generally. Fig. 7 shows that the relation of erosion thresholds with growth rate is not strict: some of the amorphous coatings also show a remarkable erosion resistance. (An x-axis value of 1 means a growth rate of 1 nm/s on 7.5 cm^2, at d_{n-s} = 5 cm). Finally fig. 8 shows that Raman spectroscopy gives an indication for the probable coating thermal shock resistance to be expected.

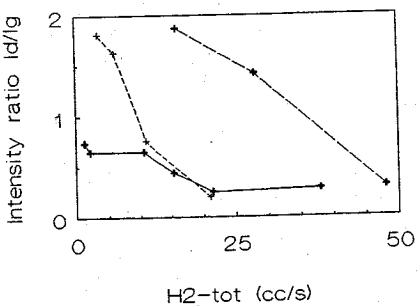

Figure 5. Raman peak intensity ratio I_d/I_g vs. total H_2 input. -+-, -+- CFC, -+- Steel; Q ≃ 60, 3 and 7.10^{-6} W^{-1} resp.

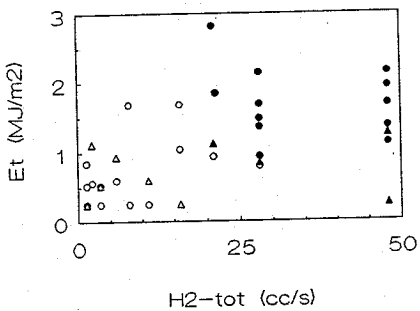

Figure 6. Erosion threshold E_t vs. total H_2 input (various other deposition parameters); • CFC, ▲ Steel.

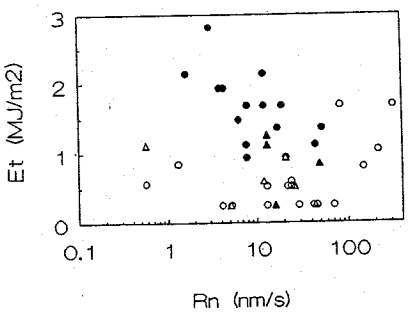

Figure 7. Erosion threshold E_t vs. normalized growth rate (various other deposition parameters; • CFC, ▲ Steel.

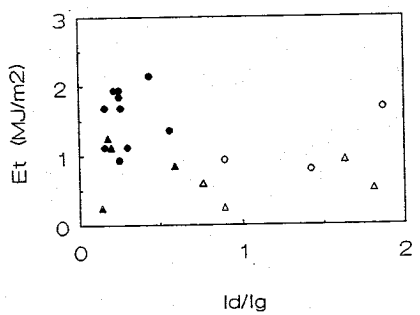

Figure 8. Relation between Raman intensity ratio I_d/I_g and erosion threshold E_t; • CFC, ▲ Steel.

CONCLUSIONS

Relations between deposited material and the deposition conditions have been established. The three diagnostics SEM, Raman spectroscopy and laser thermal shock testing give consistent results: For a coherent layer of crystalline graphite the following conditions are essential: a high (atomic) hydrogen/argon ratio of ~ 0.8, a high C_2H_2 flow rate and a substrate temperature of ~1000 °C. Coatings of amorphous graphite with a thickness of hundreds of microns and crystalline coatings with a thickness of tens of microns have been produced on areas of several cm^2, several of them having an erosion threshold of 1.7 MJ/m^2 or more. Raman spectroscopy is a fast method to get a first impression on the coating quality.

ACKNOWLEDGEMENTS

This work was part of the NET Garching - ECN Petten - TU Eindhoven research agreement (under NET contract-no. 90-237). It is funded by the Commission of the European Communities, which is representing the European Atomic Energy Community, and by Euratom/FOM Association. The authors would like to thank M.J.F. van de Sande for the technical support, and Dr. D.J. Stufkens and Mr. T.L. Snoeck of the University of Amsterdam for measuring the Raman spectra.

REFERENCES

1 G.M.W. Kroesen, D.C. Schram and M.J.F. van de Sande, Plasma Chem. and Plasma Proc., 10, 1, p. 49 (1990).

2 P.K. Bachmann, H. Lydtin, D.U. Wiechert, J.J. Beulens, G.M.W. Kroesen, D.C. Schram, Proc. 3rd Conf. on Surface Modification Technologies, p. 69, Neuchatel, Switzerland (sept. 1989).

3 A.J.M. Buuron, J.J. Beulens, M.J.F. van de Sande and D.C. Schram, Fusion Technology (july 1991), in press.

4 J.G. van der Laan, H.T. Klippel, J. Bakker, R.C.L. van der Stad, paper presented at the 4th International Conference on Fusion Reactor Materials, Kyoto, December 4-8 1989, to be published in the Journal of Nuclear Materials.

5 G.M.W. Kroesen, Ph. D. Thesis, Eindhoven University of Technology, The Netherlands (1988).

6 R. J. Nemanich and S.A. Solin, Phys. Rev. B, 20, 2, p. 392. (1979).

7 F. Tuinstra and J.L. Koenig, J. Chem. Phys., 53, p. 1126 (1970).

8 W. Zhu, C.A. Randall, A.R. Badzian, R. Messier, J. Vac. Sci. Technol. A7 (3), p. 2315, (May/Jun 1989).